A KALMAN FILTER FOR STATE ESTIMATION OF A POWER CONTROL UNIT

J. Rosenberg* , O. Bertram*
* Deutsches Zentrum für Luft- und Raumfahrt e.V., Institut für Flugsystemtechnik, Lilienthalplatz 7, 38108 Braunschweig, Deutschland

Abstract

This work deals with a Kalman filter for state estimation of a Power Control Unit (PCU) as part of a high-lift actuation system. To estimate the unknown states of the system, a Kalman filter is developed which estimates the internal volume flow between the valve block and the hydraulic motor from the measured rotational speed of the motor. For this purpose, the underlying PCU model is transferred to a state space representation and implemented in real time on DLR's A320 PCU test bench. In a measurement campaign the resulting Kalman filter was extensively tested with a total of 760 test points. The estimated flow is compared with measurement data. The Kalman filter shows consistently good results, both qualitatively and quantitatively.

Keywords

State Estimation, High-lift actuation system, Kalman filter, Virtual testing, Power control unit

NOMENCLATURE

Symbols

$\underline{A}$	System matrix	-
$\underline{B}$	Input matrix	-
$\underline{C}$	Output matrix	-
C_H	Hydraulic capacity	m^2/N
d_n	Total speed proportional viscous friction	Nms
dQ_V	Time derivation of valve flow	m^3/s^2
$\underline{D}$	Feedthrough matrix	-
D_V	Valve damping ratio	-
E_{oil}	Bulk modulus Skydrol	N/m^2
i_{ge}	PCU gear ratio	-
J_M	Total inertia	kgm^2
$\underline{K}$	Kalman gain	-
K_{LnM}	Parameter of speed dependent motor leakage	m^3
K_{LpL}	Parameter of pressure dependent motor leakage	$m^5/N/s$
M_C	Total coulomb friction	Nm
M_H	Total static friction	Nm
M_{H0}	Total static friction at 0 rpm	Nm
M_L	PCU load	Nm
M_{LM12}	Load at CDHM 1,2	Nm
M_M	Theoretical motor torque	Nm
M_R	Total friction	Nm
M_{RMpL}	Pressure dependent friction	Nm
M_{Rn}	Speed dependent friction	Nm
M_T	Torque at PCU shaft	Nm
M_V	Total viscose friction	Nm
n_{M0}	Reference speed for static friction	1/s
n_{M12}	Speed of CDHM 1,2	1/s
n_T	Speed at PCU shaft	1/s
p_A	Pressure in chamber A	N/m^2
p_B	Pressure in chamber B	N/m^2
p_L	Load pressure	N/m^2
p_R	Tank pressure	N/m^2
p_0	Supply pressure	N/m^2
$\underline{P}$	Error covariance matrix	-
$\underline{Q}$	Process noise	-
Q_{Kal}	Estimated flow with Kalman Filter	l/min
Q_{LeAB}	External leakage chamber A,B	m^3/s
Q_{Li}	Internal leakage	m^3/s
Q_{meas}	Measured flow	l/min

doi: 10.25967/550026

Q_{nom}	Valve flow at steady state	m^3/s
Q_{th}	Theoretical motor flow consumption	m^3/s
Q_V	Valve flow	m^3/s
$\underline{R}$	Measurement error covariance matrix	-
R_{pL}	Parameter load dependent friction	m^3
$\underline{u}$	Input vector	-
V_g	CDHM displacement	m^3
$\underline{x}$	State vector	-
$\underline{y}$	Output vector	-
ω_M	Angular velocity CDHM	1/s
ω_V	Eigenfrequency valve	1/s

Abbreviations

BSV	Brake solenoid valve
CDHM	Constant displacement hydraulic motor
DLR	German Aerospace Center
BSV	Extend solenoid valve
RSV	Retract solenoid valve
PCU	Power Control Unit
POB	Pressure-Off Brake
VDHM	Variable displacement hydraulic motor
VPH	Virtual Product House

1. INTRODUCTION

As part of the Virtual Product House (VPH) of the German Aerospace Center e.V. (DLR), research is being performed in the field of virtual testing. The vision of the VPH is the development of completely simulation-based methods for "virtual" certification. A high-lift system was chosen as the first application case for this. Therefore a simulation model of the high-lift system should be developed and virtual testing and certification shall be studied. In fig. 1 the A320 high-lift system can be seen. A core component of the system is the central hydrostatic drive unit, the so-called Power Control Unit (PCU).

The goal of this work is to deal with the modeling of this drive unit as well as with estimation methods to estimate unknown states with the help of measurement data. This will lead to a deeper understanding of the PCU. Furthermore the results and the knowledge shall be used, to build a simulation model for the use in virtual testing.

In chap. 2, a mathematical model of a PCU, which is still installed in the A320 family, is created. During the process, the valve block was identified as a

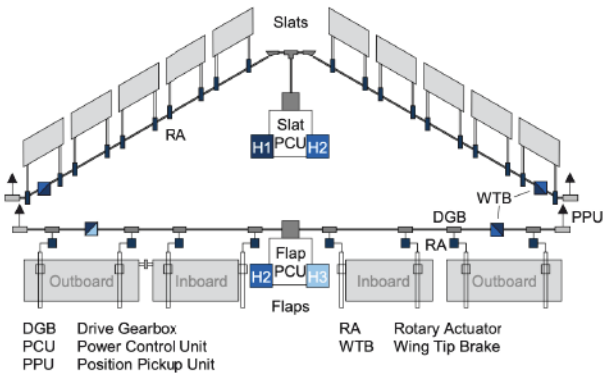

FIG 1. Airbus A320 high-lift actuation system [1]

complex component which cannot be modeled easily by physical laws. Therefore, a surrogate model of the valve block is developed. The flow plays a key role in the general operation and performance of the PCU and is hard to measure.

In order to estimate the flow rate, in sect. 2.4, a state estimation method using a Kalman filter is developed to estimate in real time the system states that cannot be measured. Therefore the mathematical model is transferred into state space representation. To evaluate the quality of the method, the flow is measured as a reference. By comparing estimated and measured flow, the Kalman filter can be evaluated. For this purpose, a PCU test bench is available. Besides the measurement of the flow, the test bench provides the rotational speed of the PCU output shaft, which serves as an input variable for the Kalman filter. In chap. 3 the test bench is introduced and the implementation of the Kalman filter is described. Chap. 4 presents the results before the work is summarized in chap. 6.

2. MATHEMATICAL MODEL OF THE POWER CONTROL UNIT

In the Airbus A320 family slats and flaps are actuated by two independent drive systems (see fig. 1). Each drive systems features a PCU which consists of a redundant set of Constant Displacement Hydraulic Motors (CDHM). The CDHMs are connected by a differential and reduction gearbox. Both PCUs are powered by three independent hydraulic reservoirs (H1,H2,H3). If one hydraulic reservoirs fails, the PCU runs at half speed. Once the final flap position is reached, the system is held in place by the Pressure-Off Brake (POB). [1] [2]

The rotational speed of the CDHMs are controlled by valve blocks. The valve block consist of a 6/5-way main control valve and three 3/2-way solenoid valves. Two solenoid valves control the main control valve, which realizes two discrete speeds and reverse rotation. The flow through the main control valve is pressure controlled by the main control spool. In addi-

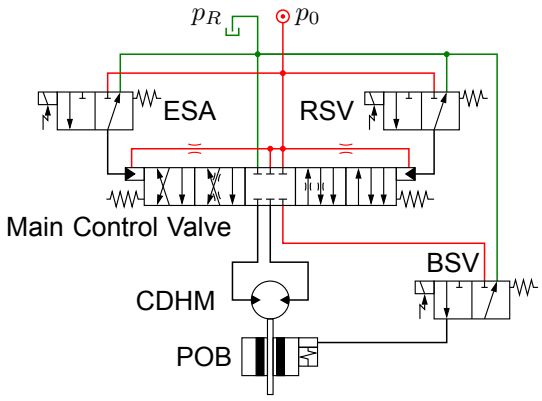

FIG 2. Hydraulic circuit diagram of a PCU drive train according to [2]

tion, the main control valve includes a throttle to drain fluid. The third solenoid valve controls the POB. Fig. 2 shows the hydraulic circuit diagram for a PCU drive train. [2] [3]

2.1. Valve block

The valve block with its components is a highly complex system. It would be challenging to model the component using white box modeling [4]. In particular, parameters such as dimensions, spring constants and pressure loss coefficients are missing and are not readily accessible.

Instead the valve block is modeled as a second-order system, based on work of [4]. In [2] and [5] the dynamics of the valve spools in their models is also described by second-order systems. Therefore an approach is used where the flow of the valve block is modeled with a PT_2-element.

$$\ddot{Q}_V + 2D_V\omega_V\dot{Q}_V + \omega_V^2 Q_V = Q_{nom}\omega_V^2 \tag{1}$$

In this representation Q_V is the valve flow while Q_{nom} is the steady state flow. D_V is the damping ratio and ω_V the eigenfrequency of the valve.

2.2. Constant displacement hydraulic motor

The modelling of a CDHMs is divided into a hydraulic and a mechanical power part [2].

2.2.1. Hydraulic modelling

The CDHM contains nine pistons which reciprocate within their respective cylinder chamber. In CDHMs the pressure difference between the chambers generates the torque on the output shaft, therefore the pressure in the cylinder is modeled. For modelling simplicity, the nine chambers are treated as only two chambers. The pressure difference between the two chambers is the load pressure, corresponding to the torque on the output shaft. Eq. 2 describes the pressure when the chamber is filled (p_A) while eq. 3 represents the pressure when the chamber is drained (p_B) [6].

$$\dot{p}_A = \frac{E_{oil}}{V_g}(Q_V - Q_{Le\,A,B} - Q_{Li} - Q_{th}) \tag{2}$$

$$\dot{p}_B = \frac{E_{oil}}{V_g}(-Q_V - Q_{Le\,A,B} + Q_{Li} + Q_{th}) \tag{3}$$

The volume flow equations expresses the conservation of mass in the two cylinder chambers. Here, Q_V describes the inflow or outflow between the valve block and the hydraulic motor. Q_{Li} describes the pressure- and speed-dependent leakages between the motor chambers and $Q_{Le\,A,B}$ the external leakages. $Q_{th} = V_g\omega_M/2\pi$ represents the theoretical motor volume flow rate. $C_H = V_g/E_{oil}$ is the hydraulic capacity of the displacement. V_g describes the geometric displacement volume of the hydraulic motor and is taken from the manufacturer's data sheet. For the bulk modulus E_{oil}, the temperature and pressure dependency is neglected [2]. Subtracting eq. 3 from eq. 2 gives the load pressure p_L in eq. 4.

$$\dot{p}_L = \frac{2}{C_H}Q_V - \frac{2K_{LpL}}{C_H}p_L - \left(\frac{2}{C_H}\cdot\frac{K_{LnM}+V_g}{2\pi}\right)\omega_M \tag{4}$$

2.2.2. Motor dynamics

The rotational speed of the motor ist caused by the sum of momentums. Therefore the motor dynamics is described with the principle of angular momentum in eq. 5. $M_M = (V_g p_L)/2\pi$ is the theoretical motor torque caused by the load pressure, M_R are the total losses or friction torques and M_{LM} is the load torque, acting on the hydraulic motor.

$$J_M\ddot{\varphi} = J_M\dot{\omega}_M = M_M - M_R - M_{LM} \tag{5}$$

The speed-dependent frictional torques are composed of viscous (M_V), Coulomb (M_C) and static friction losses (M_H). The parameters of the CDHM and the drivetrain are combined, so that eq. 6 describes the total speed-dependent frictional torques.

$$M_{Rn} = M_H + M_C + M_V = \operatorname{sign}(\omega_M)\left(M_{H0}\mathrm{e}^{-\left|\frac{\omega_M}{2\pi n_{M0}}\right|} + M_C\right) + \frac{d_n\omega_M}{2\pi} \tag{6}$$

The load pressure dependent friction torque of the motor is shown in eq. 7.

$$M_{RMpL} = R_{pL}\cdot p_L \tag{7}$$

Superimposing the friction moments from eq. 6 and eq. 7, the total frictional torque $M_R = M_{Rn} + M_{RMpL}$ acting on the hydraulic motor is obtained. All inserted in eq. 5 gives the angular velocity of the CDHM as a first order differential equation. The parameters of the motor model are taken from [2].

2.3. Differential gearbox

The PCU gearbox is a speed-summing, reducing planetary gearbox. The speed of the output shaft (n_T) is the arithmetic mean of the two motor speeds (n_{M1} and n_{M2}). [2]

$$n_T = \frac{1}{2i_{Ge}}(n_{M1} + n_{M2}) \tag{8}$$

In contrast to the speed ratio, the torque ratio is independent of normal operation or fault conditions. If one motor fails, the torque applied to the PCU output shaft is provided by the other motor. [2]

$$M_{LM1} = \frac{M_T}{2i_{Ge}} \quad \text{und} \quad M_{LM2} = \frac{M_T}{2i_{Ge}} \tag{9}$$

2.4. Kalman filter

The goal of this work is to estimate the flow of the valve by the speed of the CDHM. Therefore, a method was needed to estimate the flow using measured data. For this purpose a setup with a Kalman filter has been chosen. The Kalman filter is a proven tool to estimate system states, which are difficult to access. To validate the estimated flow, the flow of the valve was measured. First the underlying model of the Kalman filter is transferred to state space representation. After that, the equations of the discrete Kalman filter are shown and explained.

2.4.1. State space representation

The combination of eq. 1, 4 and 5 results in the following system states: The angular velocity of the CDHM (ω_M), the load pressure (p_L), the valve flow (Q_V) and the first derivative of the valve flow (dQ_V).

The angular velocity of the hydromotor ω_M is the first state described by a first order ordinary differential equation (ODE) (eq. 5). The only nonlinearity in eq. 1-9 is given in eq. 5 by the static friction component. However this component can be safely neglected because of the fact that this term becomes 0 for $\omega_M \gg 0$. The remaining equations are linear, and can be easily converted to the respective state space representation.

The ODE of the flow through the valve block was described in sec. 2.1 with eq. 1, as a second order linear ODE. The second order linear ODE was transformed into its correlating state-space equation. Therefore, the second order linear ODE is expressed by two first order linear ODEs [7]. Since there is a strong relationship between flow and speed in hydro motors, D_V and ω_V are estimated from speed measurement data.

The whole state space representation is presented in eq. 15 in the appendix. The state vector contains the above mentioned states $\underline{x} = (\omega_M, Q_V, p_L, dQ_V)^T$. Since ω_M is measured, it is the output of the system. The load acting on the drivetrain, the Coulomb friction losses and the nominal flow through the valve are the inputs to the system $\underline{u}$.

2.4.2. Time discrete Kalman filter

To run the Kalman filter in real time on the test bench hardware, the discrete Kalman filter is used. The discrete Kalman filter is determined by eq. 10 to 14 [7]. Thereby eq. 10 and 11 calculate the predicted states and covariance matrix based on the model.

$$\hat{\underline{x}}(k+1) = \underline{A}_d \cdot \tilde{\underline{x}}(k) + \underline{B}_d \cdot \underline{u}(k) \tag{10}$$

$$\hat{\underline{P}}(k+1) = \underline{A}_d \cdot \tilde{\underline{P}}(k) \cdot \underline{A}_d^T + \underline{Q}(k) \tag{11}$$

On the other hand, eq. 12, 13 and 14 update the predicted states by the measurement. Here *tilde* describes the updated, *hat* the predicted values and the indice *d* defines the discretized matrices.

$$\underline{K}(k) = \hat{\underline{P}}(k) \cdot \underline{C}^T \cdot (\underline{C} \cdot \hat{\underline{P}}(k) \cdot \underline{C}^T + \underline{R}(k))^{-1} \tag{12}$$

$$\tilde{\underline{x}}(k) = \hat{\underline{x}}(k) + \underline{K}(k) \cdot (\underline{y}(k) \tag{13}$$

$$- \underline{C} \cdot \hat{\underline{x}}(k) - \underline{D} \cdot \underline{u}(k))$$

$$\tilde{\underline{P}}(k) = (\underline{I} - \underline{K}(k) \cdot \underline{C}) \cdot \hat{\underline{P}}(k) \tag{14}$$

Matrix $\underline{A}_d$, $\underline{B}_d$ and $\underline{u}_d$ represent the discrete matrices of the simulation model from sect. 2.4.1. To connect the outputs of the system with the states, matrix $\underline{C}$, $\underline{D}$ are used. If matrix $\underline{D} = \underline{0}$, there are no inputs that directly effect the output. $\underline{P}(k)$ is the predicted covariance matrix of the estimation error and $\underline{K}(k)$ is the Kalman gain. Since the matrices do not change, the predicted covariance matrix and the Kalman gain do not change either. Matrix $\underline{Q}(k)$ and $\underline{R}(k)$ are the system noise and the measurement noise. Because the matrices do not change in this setup, the additional k will be neglected. The matrices will be described in sect. 3.2. [7]

3. TEST BENCH AND MEASUREMENT CAMPAIGN

The following chapter presents the PCU test bench and the implementation of the Kalman filter from sect. 2.4 on the dSPACE hardware. dSPACE provides hardware for real-time calculation. Here the sample time is 0.001 s. Besides the processor board, dSPACE uses I/O boards working as an interface to the test bench. Therefore dSPACE controls the test bench and records the measured data. The dSPACE hardware can be programmed with MATLAB/Simulink. Finally, the measurement campaign is explained.

3.1. Test bench setup

In order to evaluate the flow estimated with the Kalman filter, a PCU test bench with an A320 PCU is available (fig. 3). Since the PCU is used in dual-motor operation, the PCU is connected to two separate con-

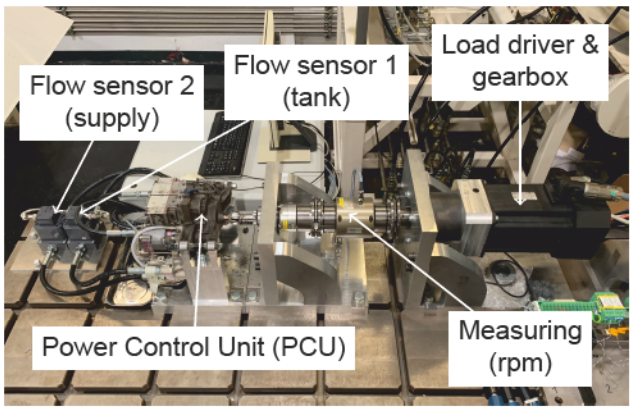

FIG 3. A320 PCU test bench

stant pressure hydraulic networks. A three-phase motor with a reducing planetary gearbox is used for load simulation. A torque measuring shaft is installed between the PCU output shaft and the electric motor. It can measure the torque and the speed during operation. The measuring shaft is connected to an analog input of the dSPACE I/O board. To measure the flow in the right-hand PCU drive train, flow sensors are installed upstream of the inlet and downstream of the outlet to the valve block. The flow is calculated from the frequency of a square signal that uses a digital input of the dSPACE I/O board. To run the PCU, the three solenoid valves of each valve block (see fig. 2) are controlled by digital outputs of the dSPACE I/O board. To control the test bench and virtualize the recorded data, the software ControlDesk is used.

3.2. Model implementation

To discretize the state space representation from sect. 2.4.1, MATLAB/Simulink is used. The model was discretized with a step size of $T_s = 0.001\,\mathrm{s}$.

The aforementioned Kalman filter was implemented in MATLAB/Simulink and then autocoded to C-code for subsequent upload onto the dSPACE hardware. This approach enables the cyclic calculation of the Kalman filter at the same frequency as the measurement data is getting sampled.

Often the measurement noise is equated to the variance of the measurement error and is usually calculated by data from a test measurement [8] [9]. With the measurement data of a speed test measurement, the empirical variance of the angular velocity is calculated. Since only one variable was measured, the covariance matrix of the measurement noise is a scalar value: $\underline{R} = s^2_{\omega_M} = 0.0337\,1/\mathrm{s}^2$.

The system noise is an abstract quantity that represents inaccuracies of the model. Mathematical models for the description of the system noise can be found in the literature. Besides models, the matrix of the system noise can be determined and improved with another Kalman filter [8]. In practice, the matrix of system noise is often fitted to the filter using the *try and error principle* [10]. This approach was chosen and the system noise was adjusted until satisfactory results were obtained. The system noise is a 4 by 4 matrix: $\underline{Q} = [1 \times 10^{-3}, 1 \times 10^{-3}, 1 \times 10^{-3}, 1 \times 10^{-3}] \cdot \underline{I}$.

Fig. 4 shows a flow chart of the Kalman filter. $\underline{u}(k)$ represents the input vector. The first component of the input vector is $(M_{LM} + M_C)$. The second component of the input vector is the volume flow at steady state Q_{nom}. Instead of estimating the volume flow at steady state and providing it as a fixed value, the volume flow at time k is the state Q_V at time $k-1$.

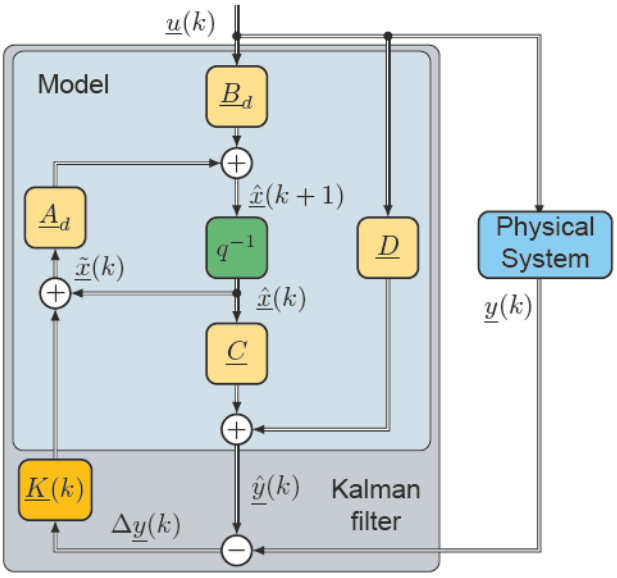

FIG 4. Flow chart of the Kalman filter according to [7]

$\underline{y}(k)$ corresponds to the input of the measured speed signal from torque measuring shaft. Before the measured values could be fed to the Kalman filter, the speed of the PCU was converted into the angular velocity of the hydraulic motors using eq. 8. After the units of the states have been converted, the data are provided to the ControlDesk interface.

3.3. Measurement campaign

In order to judge the performance of the resulting Kalman filter, a measurement campaign for different operating conditions was performed. The objective of the Kalman filter is to estimate the flow rate from the PCU speed. Therefore, the speed as well as the torque at the PCU output shaft were recorded. In order to be able to evaluate the quality of the method, the flow rate, which is used as a reference, was also measured. Since the flow rate should be investigated in both high-speed and low-speed modes, data were collected for both operating speeds.

Because the system is able to oscillate and the steady-state flow rate is of primary interest, the total time of each test sequence was set to 20 s. Of that amount, 10 s were accounted to the high-speed mode

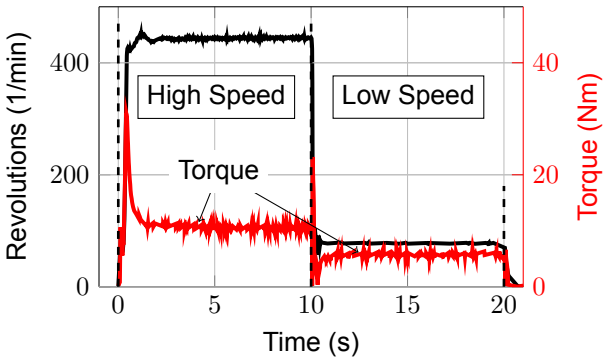

FIG 5. Measurement campaign (p_0 = 208 bar, p_R = 4 bar, $\vartheta_{Öl} = 20\,°C$, $M_L = 0$ Nm)

and the low-speed mode, respectively. Fig. 5 shows the measurement data of the torque measuring shaft from one of the test sequences.

In order to estimate the flow at many operating conditions, the flow was investigated for different supply pressures (p_0) and different load torques (M_L). For this purpose, the applied load torque was successively increased from 0 Nm to 120 Nm in steps of 4 Nm and from 120 Nm to 150 Nm in steps of 5 Nm. Furthermore, the supply pressure p_0 was increased from 154 bar to 211 bar with a step size of 3 bar. This resulted in a total of 760 test points which were all individually assessed. The tank pressure p_R was 4 bar for all measurements. To minimize variations in the material constants of the Skydrol in all measurements, the temperature of the hydraulic oil was set to $\vartheta_{oil} = 20\,°C$.

4. RESULTS

In the following section, the results of the measurement campaign are presented. For this purpose, the estimated flows are analyzed qualitatively as well as quantitatively. Finally, the measurement campaign is evaluated.

4.1. Error calculation

For the general performance of the PCU, the flow rate at steady state will be focused. First, the measured values of the flow sensor (which measures the valve inflow) Q_{meas}, and the values of the estimated valve flow from the Kalman filter (Q_{kal}), are analyzed. For the high-speed mode, the range between 3 s and 8 s is chosen, and for the low-speed mode, the data between 13 s and 18 s are analyzed. For both ranges, the arithmetic mean of the measured flow and the estimated flow is calculated. The index *1* indicates the range of the high-speed mode, the index *2* labels the low-speed mode.

4.2. Qualitative evaluation

This section evaluates the results qualitatively before quantitative differences are addressed in the following section.

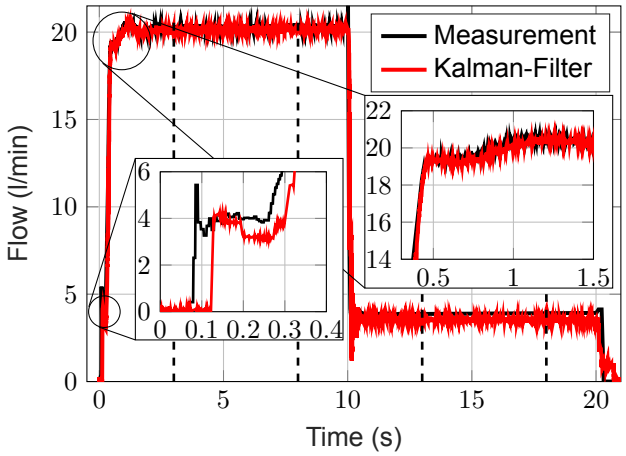

FIG 6. Flow Kalman filter and measurement (p_0 = 208 bar, $M_L = 0$ Nm)

In fig. 6 the flow curves for a supply pressure of 208 bar without load torque can be seen. With respect to the entire measurement period, it is noticeable that the Kalman filter reproduces the flow well. Especially the characteristic at the start of the PCU and the transition to the low-speed mode is correctly reproduced with respect to the measurement. In the range from 0.075 s to 0.25 s a constant flow can be recognized in the measurement data. The reason for this is the bushing of the main control spool, which is designed in a way, that there is constant flow (here 4 l/min) for a short period of time during opening. As a result the speed is also constant. This dampens the load peaks in the transmission system during acceleration [2].

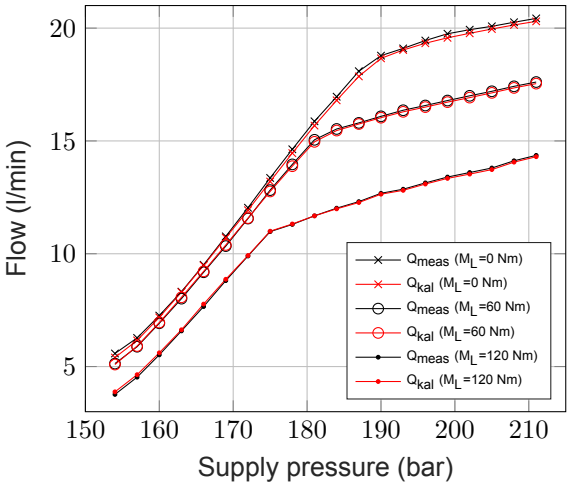

FIG 7. Flow for different load torques (high-speed mode)

This PCU specific function is not included in the model. By balancing the covariance matrix of the sys-

tem noise and the measurement noise, a simplified model can be compensated by good measurement data. Here, the measurement is dominating, which results in a better representation of the flow. When the flow changes rapidly, the estimated flow of the Kalman filter follows the measured values. This results in a time delay between flow and rotational speed, as one variable is caused by the other.

In fig. 7, the measured and estimated flows for different load torques are shown for the high-speed mode. The curves of the flow can be roughly divided into two regions depending on the supply pressure. The curves at low pressure look like a quadratic relationship, which changes to a linear curve above a certain pressure. The point where one curve changes into the other, depends on the load torque. For an example load torque of 0 Nm, the pressure where the curve changes is 190 bar. For 60 Nm, the pressure is 181 bar, and for 120 Nm, the pressure decreases to 175 bar. Even the measured and estimated values differ, the qualitative profile remains the same.

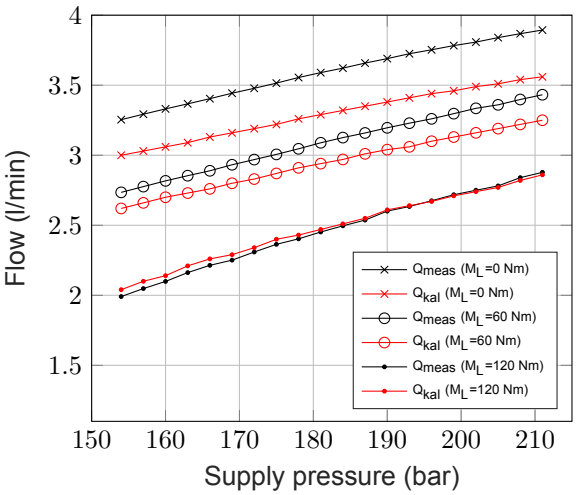

FIG 8. Flow for different load torques (low-speed mode)

Fig. 8 shows the measured and estimated flows for different load torques at low-speed mode. Compared to the flows of the high-speed mode, the curves are approximately linear. Depending on the load torque, the flow curves have a different gradient. Compared to the curves of the high-speed mode in fig. 7, the differences between the estimated and the measured values are particularly noticeable. Looking at the results of the Kalman filter, the deviations become smaller with increasing load torque.

4.3. Quantitative evaluation

To capture the quantitative differences, the deviation of the estimated value to the measured flow was calculated. It was differentiated whether the measured value is overestimated or underestimated.

Over the whole measurement campaign in high-speed mode, the biggest error was in the range of $-0.23\,\mathrm{l/min}$ ($p_0 = 187\,\mathrm{bar}$ and $M_L = 0\,\mathrm{Nm}$) to $0.17\,\mathrm{l/min}$ ($p_0 = 157\,\mathrm{bar}$ and $M_L = 145\,\mathrm{Nm}$), while biggest relative error was recorded to be $-3.2\,\%$ ($p_0 = 154\,\mathrm{bar}$ and $M_L = 0\,\mathrm{Nm}$) to $4.2\,\%$ ($p_0 = 157\,\mathrm{bar}$ and $M_L = 145\,\mathrm{Nm}$).

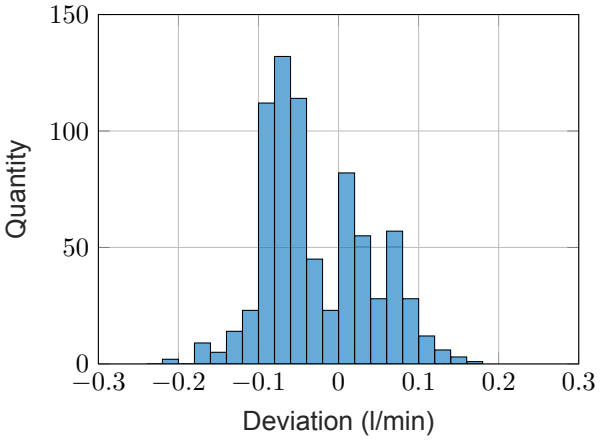

FIG 9. Histogram of the deviations (high-speed mode)

Through the entire measurement campaign the largest deviations occur in similar operating points. First of all, the largest deviations occur at low supply pressures. Secondly, the measured flow is underestimated at low load torques and overestimated at high torques. Further on, the distribution of the deviations will be examined in more detail in order to better evaluate the correct working of the Kalman filter. In fig. 9 the deviations are shown in a histogram with a class width of $0.02\,\mathrm{l/min}$.

TAB 1. Average deviations in l/min (high-speed mode)

Kalman-Filter	$\overline{Q}_1$	σ_{Q_1}	$\overline{\lvert Q_1 \rvert}$	$\sigma_{\lvert Q_1 \rvert}$
High speed	-0.025	0.063	0.060	0.035

The Kalman filter tends to underestimate the measured value. This is also expressed by the mean value ($-0.025\,\mathrm{l/min}$) and the standard deviation of the deviations ($0.063\,\mathrm{l/min}$). Determining the mean for the absolute deviations, we obtain $0.060\,\mathrm{l/min}$ with a standard deviation of $0.035\,\mathrm{l/min}$. The mean value is no longer corrected by the different signs. The results are summarised in tab. 1.

Similar to the high-speed mode, the deviations for the low-speed mode are analyzed quantitatively. Over the whole measurement campaign in low-speed mode, the biggest error was in the range of $-0.33\,\mathrm{l/min}$ ($p_0 = 205$, 208 and 211 bar and $M_L = 0\,\mathrm{Nm}$) to $0.12\,\mathrm{l/min}$ ($p_0 = 163$ and 169 bar and $M_L = 155\,\mathrm{Nm}$), while the biggest relative error was recorded to be $-8.6\,\%$ ($p_0 = 205\,\mathrm{bar}$ and $M_L = 0\,\mathrm{Nm}$) to $6.8\,\%$ ($p_0 = 163\,\mathrm{bar}$ and $M_L = 155\,\mathrm{Nm}$).

Considering the deviations at low-speed mode over the entire measurement campaign, the largest deviations occur again at similar operating points. The

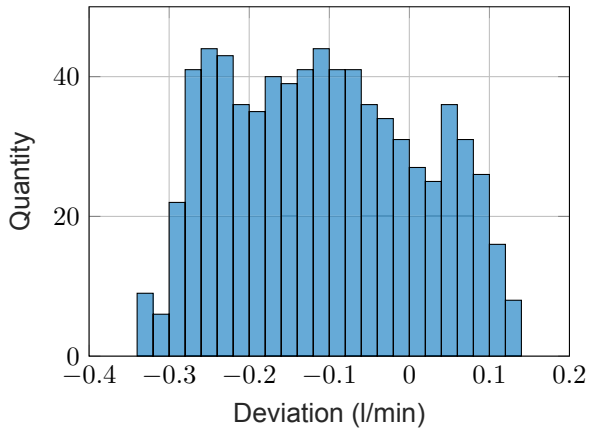

FIG 10. Histogram of the deviations (low-speed mode)

largest underestimated deviations occur at low load torques and high supply pressures (see fig. 8). In contrast, the measured value is overestimated at low supply pressures and high load torques.

In chap. 2 the system behavior of the valve block was described in detail. Especially the low-speed mode is achieved by a complex pressure equilibrium at the main control spool, where hydraulic fluid is also discharged via a throttle [2]. This particular behavior is not modeled and could be a possible explanation for the worse flow estimation at low-speed mode. Because some hydraulic fluid is drained within the valve block, this part of the fluid never reaches the CDHM. Therefore the flow measurement might not be the correct reference.

Next, the distribution of the deviations is investigated in more detail. In fig. 10 the deviations are plotted as a histogram with a class width of 0.02 l/min. This clearly shows that the flow rate is mostly underestimated. This is also indicated by the mean value. The mean deviation is −0.11 l/min with a standard deviation of 0.11 l/min. On the other hand, if we consider the mean value of the absolute value of the deviations, we obtain 0.13 l/min with a standard deviation of 0.090 l/min. The characteristic values are shown in tab. 2.

TAB 2. Average deviations in l/min (low-speed mode)

Kalman-Filter	$\overline{Q}_2$	σ_{Q_2}	$\overline{\lvert Q_2 \rvert}$	$\sigma_{\lvert Q_2 \rvert}$
Low speed	−0.11	0.12	0.13	0.090

5. CONCLUSION

The data of one complete measurement cycle are shown in fig. 6 and were described. The constant flow during acceleration of the PCU is captured. Even if a simple model is used, the Kalman filter is able to achieve a good estimation. Given this objective, the Kalman filter can deemed to be very effective.

For the high-speed mode, the Kalman filter provides consistently good results. The method records the flow over the entire range of the measurement campaign. The qualitative characteristic of the flow is estimated correctly. Additionaly to the qualitative aspects, the deviations between estimated and measured flows were considered. In general, the Kalman filter tends to underestimate the measured values. This might be caused by the constant parameters used in the motor model. This leads to worse results, especially off the operating point.

In addition to the high-speed mode, the PCU was also investigated at low-speed mode. Looking at the general course of the estimated flow rates, the Kalman filter correctly reproduces the course. The dependence of the flow on supply pressure and load torque is correctly reflected. Nevertheless, compared to the high-speed mode, the results are less good. This is especially shown by the direct comparison of fig. 7 and fig. 8. The discrepancies between the measured and estimated flows are much more noticeable. This suggests that the physical effects are better represented in the high-speed mode or the measured flow is not the correct reference. The deviations were also examined for the low-speed mode. Similar to the high-speed mode, the Kalman filter underestimates the measured value more often.

Finally, the following conclusions can be drawn:

- The flows estimated for the high-speed mode are better compared to the low-speed mode.
- The Kalman filter tends to underestimate the measured values.
- The Kalman filter can represent unknown effects and estimate the flow in detail due to a good balance between measurement and model influence.

6. OUTLOOK

The goal of this paper was to estimate the flow rate of a central hydrostatic drive unit for a high-lift system, also called power control unit (PCU). This was achieved with a Kalman filter, that used the rotational speed of the CDHM as an input. The Kalman filter was evaluated on a test bench, where the hydraulic flow could be measured. The flow measurement was the reference to evaluate the estimated flows qualitatively as well as quantitatively. For the Kalman filter the mathematical model was transferred to state space representation and a discrete Kalman filter was developed. The Kalman filter runs in real time on the test bench hardware. The obtained results can be summarized the following way:

- Modeling the valve block with a PT_2-element is suitable for estimating the flow using measured data.
- Overall, the flow was estimated qualitatively as well as quantitatively in a good way
- The Kalman filter estimates flow better for the high-speed mode compared to the low-speed mode and provides the ability to compensate a simplified model.

Furthermore the valve block might be investigated in detail. Especially the drained flow at low-speed mode shall be further examined. Such a characterization might improve the estimation performance. Also it can be investigated if the measured flow at low-speed is the correct reference for the Kalman filter.

The knowledge gained about the flow can be used to create a (semi-) physical model of the valve block. Furthermore the PCU model can also be expanded to add a variable displacement hydraulic motor (VDHM) which are currently used in modern aircraft e.g. the Airbus A350. These models can be used in the high-lift system for the VPH project for virtual testing. Here, the effect of different flows on system requirements, such as the positioning behavior of the flaps and the actuation time, can then be evaluated.

Acknowledgment

The Virtual Product House (VPH) is funded through a start-up project by the state of Bremen and the European Regional Development Fund (ERDF) as well as internal DLR project funds.

Contact address:

Jan.Rosenberg@dlr.de

References

[1] Thomas Lampl, Ralf Königsberger, and Mirko Hornung. Design and evaluation of distributed electric drive architectures for high-lift control systems. In *66. Deutsche Luft-und Raumfahrtkongress*, 2017.

[2] Gerhard Geerling. Entwicklung und Untersuchung neuer Konzepte elektrohydraulischer Antriebe von Flugzeug-Landeklappensystemen. *Ölhydraulik und Pneumatik*, 47(7):456–457, 2003.

[3] Olaf Biedermann and Gerhard Geerling. Power control units with secondary controlled hydraulic motors-a new concept for application in aircraft high lift systems. In *Recent Advances in Aerospace Hydraulics*, 1998.

[4] Sondre S. Tørdal, Andreas Klausen, and Morten K. Bak. Experimental system identification and black box modeling of hydraulic directional control valve. *Modeling, Identification and Control*, 35(4):225–235, 2015.

[5] Morten K. Bak and Michael R. Hansen. Analysis of offshore knuckle boom crane-part one: modeling and parameter identification. *Modeling, Identification and Control*, 34(4):157–174, 2013.

[6] Jaroslav Ivantysin and Monika Ivantysinova. *Hydrostatische Pumpen und Motoren: Konstruktion und Berechnung*. 1993.

[7] Reiner Marchthaler and Sebastian Dingler. *Kalman-Filter*. Springer, 2017.

[8] Greg Welch, Gary Bishop, et al. An introduction to the Kalman filter. Dept. of Computer Science Tech. Report, TR 95-041, 1995.

[9] Wolfgang Schenk, Friedrich Kremer, Gunter Beddies, Thomas Franke, Petrik Galvosas, and Peter Rieger. *Physikalisches Praktikum*. Springer, 2014.

[10] Oleksiy V. Korniyenko, Mohammad S. Sharawi, and Daniel N. Aloi. Neural network based approach for tuning kalman filter. In *2005 IEEE International Conference on Electro Information Technology*, pages 1–5. IEEE, 2005.

APPENDIX

State space model:

(15)
$$\begin{aligned}\underline{\dot{x}} &= \underline{A}\cdot\underline{x} + \underline{B}\cdot\underline{u} \quad \text{with:}\\ \underline{y} &= \underline{C}\cdot\underline{x} + \underline{D}\cdot\underline{u}\end{aligned}$$

$$\underbrace{\begin{pmatrix}\dot{\omega}_M\\ \dot{Q}_V\\ \dot{p}_L\\ \dot{dQ}_V\end{pmatrix}}_{\underline{\dot{x}}}, \quad \underbrace{\begin{pmatrix}\omega_M\\ Q_V\\ p_L\\ dQ_V\end{pmatrix}}_{\underline{x}}$$

$$\underbrace{\begin{pmatrix} -\frac{d_n}{J_M 2\pi} & 0 & \left(\frac{V_g}{J_M 2\pi} - \frac{R_{pL}}{J_M}\right) & 0\\ 0 & 0 & 0 & 1\\ -\left(\frac{2}{C_H}\cdot\frac{K_{LnM}+V_g}{2\pi}\right) & \frac{2}{C_H} & -\frac{2K_{LpL}}{C_H} & 0\\ 0 & -\omega_V^2 & 0 & -2D_V\omega_V\end{pmatrix}}_{\underline{A}}$$

$$\underbrace{\begin{pmatrix}\frac{1}{J_M} & 0\\ 0 & 0\\ 0 & 0\\ 0 & \omega_V^2\end{pmatrix}}_{\underline{B}}, \quad \underbrace{\begin{pmatrix}(M_{LM}+M_C)\\ Q_{nom}\end{pmatrix}}_{\underline{u}}$$

$$\underbrace{\omega_M}_{\underline{y}}, \quad \underbrace{\begin{pmatrix}1 & 0 & 0 & 0\end{pmatrix}}_{\underline{C}}, \quad \underbrace{\begin{pmatrix}0 & 0\end{pmatrix}}_{\underline{D}}$$